Solid-State ^{93}Nb, ^{19}F, and ^{113}Cd Nuclear Magnetic Resonance Study of Niobium Oxyfluorides: Characterization of Local Distortions and Oxygen/Fluorine Ordering

Lin-Shu Du,[†] Robert W. Schurko,[‡] Namjun Kim, and Clare P. Grey*

Department of Chemistry, State University of New York at Stony Brook, Stony Brook, New York 11794-3400

Received: February 19, 2002; In Final Form: May 28, 2002

The local structures and oxygen/fluorine ordering of $Cdpy_4NbOF_5$ (py = C_5H_5N) and $[pyH]_2[Cdpy_4(NbOF_5)_2]$ have been investigated with ^{19}F, ^{113}Cd, and ^{93}Nb solid-state NMR spectroscopy. The ^{93}Nb magic-angle spinning (MAS) NMR spectra acquired at an ultrahigh magnetic field strength (19.6 T) and at ultrahigh spinning speeds (∼43 kHz) of both compounds are dominated not only by the quadrupolar interaction but also by the chemical shielding (CS) interaction, consistent with highly asymmetric environments for niobium. A methodology is presented to extract the nuclear quadrupole coupling constant C_Q, the asymmetry parameter η, and the isotropic chemical shift δ_{iso} in the presence of a large chemical shift anisotropy (CSA). The CS tensor was then obtained from the simulations of the ^{93}Nb ($I = 9/2$) static NMR spectrum. The separations between the centerband of the central transition and sidebands of the $\pm 3/2 \leftrightarrow \pm 5/2$ satellite transition in the ^{93}Nb MAS NMR spectra are sensitive to the value of $C_Q(^{93}Nb)$, while the line shapes are mainly determined by η and the relative orientation between the electric field gradient (EFG) and CS tensors. Thus, simulations of the MAS NMR spectra provided additional constraints on the fitting of all these parameters. The ^{93}Nb MAS NMR spectra acquired at lower field and lower spinning speeds, where the spinning sidebands are not separated from the centerband, were also reproduced in the simulations. The following parameters were determined for the two compounds at room temperature: $C_Q = 36.0(5)/33.2(5)$ MHz, $\eta = 0.50(5)/0.40(5)$, $\delta_{iso}(^{93}Nb) = -1310(10)/-1320(10)$ ppm, $\Omega = 1000(20)/1100(20)$ ppm, $\kappa = 1.00(5)/0.8(1)$, $\alpha = 0(20)°/60(20)°$, $\beta = 0(2)°/5(2)°$, $\gamma = 0(20)°/0(20)°$ for $Cdpy_4NbOF_5/[pyH]_2[Cdpy_4(NbOF_5)_2]$, respectively. A very distorted multiplet in the solid-state ^{19}F MAS NMR spectra was observed, which arises from *J*-coupling [$^1J(^{93}Nb,^{19}F) = 362(2)$ and 350(5) Hz, for $Cdpy_4NbOF_5$ and $[pyH]_2[Cdpy_4(NbOF_5)_2]$, respectively] and residual dipolar coupling between the ^{19}F and ^{93}Nb nuclei. Only one ^{113}Cd NMR resonance is observed for $Cdpy_4NbOF_5$, which, together with the ^{19}F NMR, suggests that the O-substitution is not random. On the basis of the ^{113}Cd NMR, the $NbOF_5$ octahedra are most likely oriented in opposite directions in different chains so as to allow the acentric $NbOF_5$ octahedra to occupy a center of inversion in the crystal structure of this compound determined by X-ray diffraction (the "interchain" cancellation mechanism proposed by Heier et al., in *J. Solid State Chem.* **1997**, *133*, 576−579).

Introduction

The mixed metal oxyfluoroniobates, $Cdpy_4NbOF_5$ and $[pyH]_2[Cdpy_4(NbOF_5)_2]$, have been previously synthesized and characterized in order to investigate out-of-center distortions of Nb octahedra,[1,2] which are proposed to be one of the possible causes of ferroelectric behavior in niobates.[3] The out-of-center distortion is commonly seen in $NbOF_5$ octahedra[4] but is also found in NbO_6[5,6] and NbF_6 octahedra[7] and can be explained by the second-order Jahn−Teller theorem.[8] Since very little information is known regarding the effect of these distortions on the chemical shielding (CS) and electric field gradient (EFG) tensors of these distorted hexacoordinate niobium environments, they represent interesting model compounds for NMR studies.

The structures of $Cdpy_4NbOF_5$ and $[pyH]_2[Cdpy_4(NbOF_5)_2]$ are shown in Figure 1, panels a and b, respectively. $Cdpy_4NbOF_5$ consists of nonintersecting chains of alternating corner-shared $[Cd(py)_4(O/F)_{2/2}]^{0.5+}$ and $[NbF_4(F/O)_{2/2}]^{0.5-}$ octahedra, $X_{2/2}$ indicating two bridging anions. The niobium atom of $Cdpy_4NbOF_5$ was found, by X-ray diffraction, to lie on a center of inversion in the unit cell.[1] Since out-of-center distortions were expected for the $NbOF_5$ octahedra, disorder in the occupancy of the bridging anion site was proposed.[1] Similar disorder was also proposed for $CuNbOF_5{\cdot}4H_2O$.[9] $[pyH]_2[Cdpy_4(NbOF_5)_2]$ contains clusters of one $[Cd(py)_4O_{2/2}]$ octahedron corner-shared with two $[NbF_5O_{1/2}]^{1-}$ octahedra, with pyridinium (pyH^+) cations in the spaces between the clusters. $N-H^+\cdots F$ hydrogen bonding was proposed to link the pyridinium ion to the $NbOF_5$ octahedron in the clusters.[2] A displacement of Nb toward O in the F−Nb−O axis of the $NbOF_5$ octahedron was seen, a difference in bond lengths between Nb−O and Nb−F of 0.35 Å being observed.[2]

In this paper, we report the use of ^{93}Nb (spin 9/2), ^{19}F (spin 1/2), and ^{113}Cd (spin 1/2; natural abundance = 12.26%) magic-angle spinning (MAS) NMR to study the niobium local environments and fluoride-ion order in the niobium oxyfluorides. The nuclear quadrupole moment, *eQ*, is extremely large for the 100% naturally abundant nucleus ^{93}Nb [$Q(^{93}Nb) = -0.22 \times 10^{-28}$ m^2],[10] and thus ^{93}Nb NMR represents an ideal probe of small distortions in the local environment of the niobium atom.

* To whom correspondence should be addressed: Phone 631-632-9548; fax 631-632-5731; e-mail cgrey@notes.cc.sunysb.edu.

[†] Present address: Department of Geological and Environmental Sciences, Stanford University, Stanford, CA 94305-2115.

[‡] Present address: Department of Chemistry and Biochemistry, School of Physical Sciences, University of Windsor, Windsor, Ontario, Canada N9B 3P4.

10.1021/jp020457q CCC: $22.00
Published on Web 07/31/2002

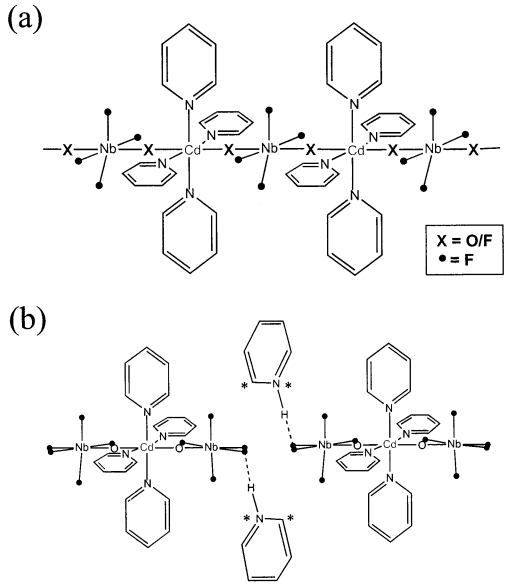

Figure 1. Structures of (a) $Cdpy_4NbOF_5$ and (b)$[pyH]_2[Cdpy_4(NbOF_5)_2]$. Asterisks are used to label the two sites in (b) that are partially occupied by both C and N, reflecting the disorder in the orientation of the pyridinium ions.

Our previous ^{19}F MAS NMR studies of a series of oxyfluorides have demonstrated the sensitivity of this nucleus to fluorine local order.[11] In this paper, both ^{113}Cd and ^{19}F MAS NMR are used to test the proposals for long-range ordering of the anions in the Nb−O/F−Cd−O/F− chains of $Cdpy_4NbOF_5$. The ^{93}Nb, ^{19}F indirect spin−spin coupling (*J*-coupling), ^{93}Nb, ^{19}F and ^{19}F, ^{19}F direct dipolar coupling, ^{93}Nb quadrupolar interaction, and ^{93}Nb chemical shielding anisotropy (CSA) are all probed with ^{93}Nb and ^{19}F NMR to characterize the local structure surrounding the niobium atoms.

The ^{93}Nb spectra are usually dominated by the quadrupolar interaction and even the resonance from the central transition ($|-1/2\rangle \leftrightarrow |+1/2\rangle$) is typically very broad. A combination of high magnetic fields and high MAS frequencies are required in order to extract the quadrupole coupling constants (C_Q) and the quadrupolar asymmetry parameters, η, from ^{93}Nb spectra. An approach to extract these and the CS values was reported in our earlier study of potassium heptafluoroniobate, K_2NbF_7, a system with a heptacoordinate Nb environment.[12] The spectra reported here are similarly analyzed to extract values for the ^{93}Nb quadrupolar and chemical shift tensors, to relate the size and relative orientation of these tensors to the niobium local coordination environments. Now, however, the effect of the much larger CSA needs to be considered in the analysis. The $^1J(^{93}Nb,^{19}F)$ coupling was also measured. *J*-couplings are typically unobservable in the ^{19}F MAS NMR spectra due to line broadening caused by the large fluorine homonuclear dipolar couplings. However, our previous experiments on K_2NbF_7 and α- and β-PbF_2 have shown that direct one-bond *J*-couplings can sometimes be observed when fast MAS frequencies are used.[12−14]

Experimental Section

Sample Preparation. Samples were synthesized by Dr. K. R. Heier in Professor K. R. Poeppelmeier's group at Northwestern University. Details of the synthesis can be found elsewhere.[1,2]

NMR Measurements. Solid-state ^{19}F MAS NMR spectra were obtained with wide-bore Chemagnetics CMX-200 (4.7 T) and CMX-360 (8.5 T) spectrometers at operating frequencies of 188.33 and 338.76 MHz, respectively, with $\pi/2$ pulses of 1.8−2.4 μs and recycle delays of 10−20 s. A Chemagnetics 3.2 mm double-resonance probe capable of reaching spinning frequencies of 24 kHz with a reduced ^{19}F background signal was used on both spectrometers for the acquisition of ^{19}F MAS NMR spectra. Solid-state ^{113}Cd MAS NMR spectra were obtained with a Chemagnetics 3.2 mm double-resonance probe with a CMX-360 spectrometer at an operating frequency of 79.84 MHz with a $\pi/2$ pulse of 4.0 μs, a recycle delay of 100 s, and the collection of ∼2400 transients. Solid-state ^{93}Nb NMR spectra were obtained with the CMX-360 spectrometer and a narrow-bore Bruker AMX-833 (19.6 T) spectrometer at operating frequencies of 87.99 and 203.44 MHz, respectively. The Chemagnetics 3.2 mm double-resonance probe was used for the acquisition of ^{93}Nb MAS NMR spectra at 8.5 T, with radio frequency (rf) field strengths of 120 kHz, effective 90° pulse widths of 0.6 μs measured on an actual solid sample ($\pi/10$ when measured with the solution standard), pulse delays of 0.5 s, and 50 000−270 000 transients. Due to relatively long pulse rise times on the order of 0.2−0.4 μs, it was not possible to use any shorter pulses, to optimize the excitation of the entire central transition line shape. The ^{93}Nb static spectra at 8.5 T were collected with a Chemagnetics 5.0 mm triple-resonance probe (for improved signal-to-noise ratio, S/N) with rf field amplitudes of ∼80 kHz, pulse widths of 0.9 μs, pulse delays of 0.4 s, and 220 000−320 000 transients. An ultrafast MAS probe, designed and built by Ago Samoson and Tiit Tuherm at National Institute of Chemical Physics and Biophysics,[15] that uses ∼2.0 mm rotors that can reach spinning speeds of 50 kHz, was used for the acquisition of ^{93}Nb MAS spectra at 19.6 T with an rf field amplitude of 200 kHz, pulse widths of 1.5 μs, and pulse delays of 0.3 s and 20 000 to 28 000 transients. The chemical shifts of ^{19}F, ^{113}Cd, and ^{93}Nb are referenced to $CFCl_3$, aqueous $Cd(ClO_4)_2$, and $NbCl_5$ in CH_3CN, respectively (all at 0.0 ppm).

NMR Simulations. The central transition of the ^{93}Nb MAS NMR spectra acquired at 19.6 T, the ^{93}Nb static NMR spectra acquired at 8.5 T, and the ^{19}F MAS spectra acquired at 4.7 T were simulated by use of WSolids, which was developed by Klaus Eichele at Dalhousie University. WSolids utilizes the space-tiling algorithm of Alderman et al.[16] for rapid generation of powder spectra. The ^{93}Nb MAS spectra acquired at 8.5 and 19.6 T were simulated numerically by use of an efficient time propagation algorithm based on Floquet theory.[17,18] Programs were written in the C++ programming language, with the GAMMA platform[19] for simulation of NMR spectra, and were developed by Kwang Hun Lim at SUNY Stony Brook.

Results and Discussions

Fluorine-19 MAS NMR. The ^{19}F MAS NMR spectra of $Cdpy_4NbOF_5$ obtained at a spinning speed of 24 kHz at 4.7 and 8.5 T (Figure 2, spectra a and b, respectively) show a resonance at ca. −145 ppm and a peak with very asymmetric line shape centered at ca. 30 ppm. Since the intensity ratio for the −145:30 ppm resonances (about 1:4) is the same as the multiplicity ratio of the axial to equatorial fluoride ions, these resonances are assigned to the bridging (axial) and equatorial fluorine atoms in the $NbOF_5$ octahedron, respectively. A multiplet was observed for the resonance of the equatorial F in the spectrum collected at 4.7 T and is due to $^1J(^{93}Nb,^{19}F)$ coupling. Since ^{93}Nb is a spin 9/2 nucleus, 10 peaks should be observed in the spin 1/2 spectrum. Unlike solution NMR, these 10 peaks are no longer evenly spaced, due to the presence of residual dipolar coupling between the niobium and fluorine

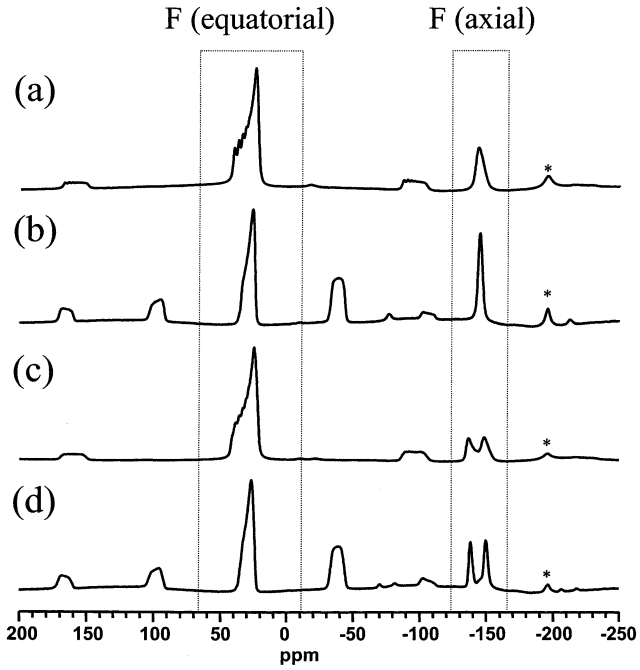

Figure 2. ^{19}F MAS spectra of $Cdpy_4NbOF_5$, collected at (a) 4.7 T and (b) 8.5 T, and of $[pyH]_2[Cdpy_4(NbOF_5)_2]$ collected at (c) 4.7 T and (d) 8.5 T, at spinning speeds (ν_r) of 24 kHz. Asterisks denote small impurity peaks. The dotted rectangular boxes represent the centerbands originating from the equatorial and axial fluorine sites shown in Figure 1.

nuclei.[12] The spacings between the peaks in Figure 2a decrease slightly from high to low frequency, the peaks broadening in this direction as well. The *J*-coupling constant can be obtained by simulating the multiplet pattern; this will be discussed later. Due to the larger field inhomogeneity and chemical shift distribution (in hertz) at the higher field (8.5 T), the 10 peaks overlap, resulting in an asymmetric line shape but no resolved multiplet (Figure 2b). Since no resolved multiplet was observed for the −145 ppm resonance, even in the spectrum collected at the lower field (4.7 T), *J*-coupling between the bridging F and Nb must be smaller. This may result from the longer Nb−F(axial) bond (2.10 Å) in comparison to the Nb−F(equatorial) bond (1.93 Å).[2] A slightly asymmetric line shape can still be observed, however, in the spectrum collected at 4.7 T.

The ^{19}F MAS NMR spectra of $[pyH]_2[Cdpy_4(NbOF_5)_2]$ collected at 4.7 and 8.5 T (Figure 2, spectra c and d, respectively) show a peak with an asymmetric line shape at ca. 30 ppm. Surprisingly, there are two resonances, located at −138 and −150 ppm, with equal intensities. There are three crystallographically distinct F sites in $Cdpy_4NbOF_5$[1] and $[pyH]_2[Cdpy_4(NbOF_5)_2]$,[2] two (F1 and F2) in the equatorial position and one (F3) in the axial position of the $NbOF_5$ octahedron, with ratios (F1:F2:F3) of 2:2:1. Since the ratios of the peaks at ∼30, −138, and −150 ppm are 8:1:1, the broad peak at ∼30 ppm is assigned to the equatorial F (F1 and F2) and the peaks at −138 and −150 ppm are both assigned to the axial F (F3). A hydrogen-bonding interaction between the F3 and the N in pyridinium ion ($N-H^+\cdots F$) has been proposed in the earlier study.[2] The two F3 peaks are not, however, a result of *J*-coupling between ^{19}F and ^{1}H since the shift does not change with field. Single-crystal diffraction data revealed only three unique atoms in the asymmetric unit for pyridinium, indicating disorder between N and one C in the pyridinium ion[2] (Figure 1b). This may result in two different axial F environments, leading to the two resonances at around −145 ppm.

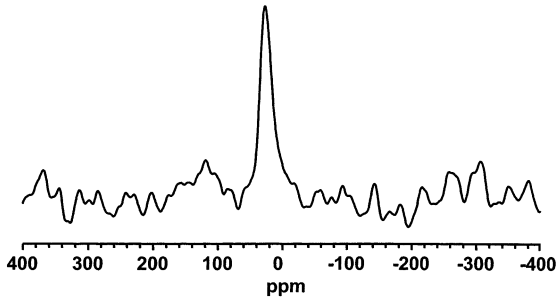

Figure 3. ^{113}Cd MAS spectrum of $Cdpy_4NbOF_5$ collected at a field strength of 8.5 T and $\nu_r = 23$ kHz.

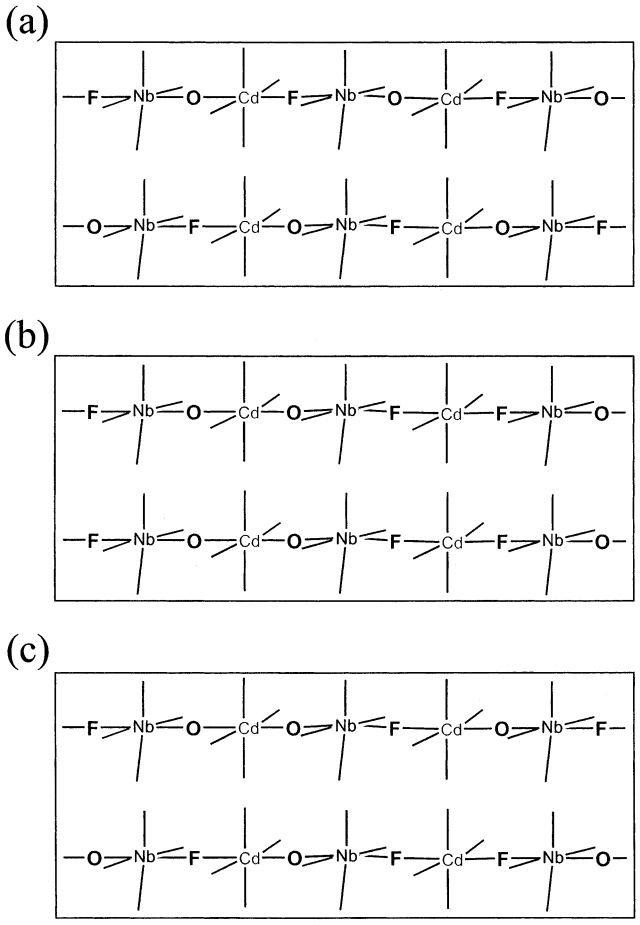

Figure 4. Three possible disorder mechanisms for $Cdpy_4NbOF_5$: an interchain cancellation (a), an intrachain cancellation (b), and a random cancellation (c) of the acentric intraoctahedral distortions.

Cadmium-113 MAS NMR: O/F Ordering in $Cdpy_4NbOF_5$. The ^{113}Cd MAS NMR spectrum of $Cdpy_4NbOF_5$ (Figure 3) shows one resonance at 27.5 ppm. Only one crystallographically distinct Cd site was refined in the X-ray study of $Cdpy_4NbOF_5$, by use of a centric space group *C*2/*c* (no. 15).[1] To generate an out-of-center distortion for the $NbOF_5$ octahedron, O/F disorder in the asymmetric unit was proposed, allowing the acentric $NbOF_5$ group to occupy an apparent center of inversion in the crystal structure.[1] This local O/F disorder can result in three possible long-range ordering schemes: interchain cancellation, intrachain cancellation, or random cancellation of acentric intraoctahedral distortions as shown in Figure 4, panels a−c, respectively. Two possible cadmium environments result from the intrachain cancellation scheme: $Cdpy_4O_2$ and $Cdpy_4F_2$. There is only one cadmium environment, $Cdpy_4OF$, in the

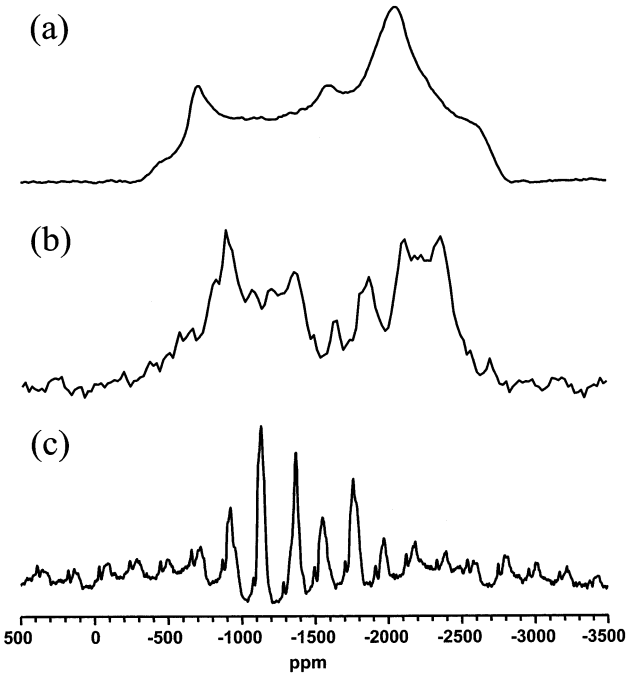

Figure 5. (a) ^{93}Nb static spectra of $Cdpy_4NbOF_5$ collected at 8.5 T, and ^{93}Nb MAS spectra of $Cdpy_4NbOF_5$ collected at (b) 8.5 T, $\nu_r = 20$ kHz, and (c) 19.6 T, $\nu_r = 43$ kHz.

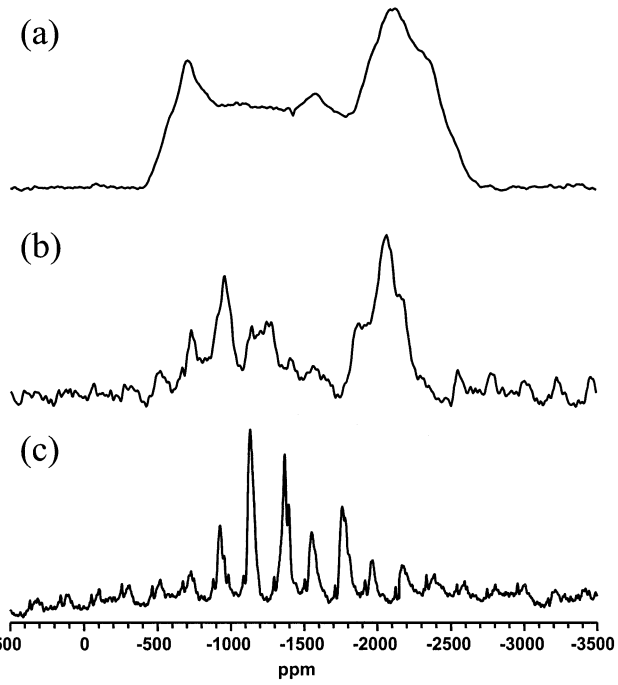

Figure 6. (a) ^{93}Nb static spectra of $[pyH]_2[Cdpy_4(NbOF_5)_2]$ collected at 8.5 T, and ^{93}Nb MAS spectra of $Cdpy_4NbOF_5$ collected at (b) 8.5 T, $\nu_r = 20$ kHz, and (c) 19.6 T, $\nu_r = 42.5$ kHz.

interchain cancellation mechanism. The random cancellation mechanism results in all three Cd environments indicated above. The observation of only one resonance in ^{113}Cd MAS spectrum is consistent with the interchain cancellation O/F ordering mechanism (Figure 4a), since the chemical shift in ^{113}Cd is expected to be extremely sensitive to the local environment of cadmium.

It is important to note that the signal-to-noise ratio of the ^{113}Cd spectrum was not very high, and it is always difficult to completely rule out the possibility that we are actually detecting a signal from an impurity phase. The ^{19}F NMR, however, provides additional support for either an interchain or an intrachain cancellation mechanism. O/F disorder due to a random cancellation mechanism (Figure 4c) will result in two local environments for ^{19}F, one involving a fluorine atom connected via Cd to another fluorine atom (a F−Cd−F local environment) and the other present in the F−Cd−O local environment.

Niobium-93 NMR. The ^{93}Nb NMR spectra of $Cdpy_4NbOF_5$ and $[pyH]_2[Cdpy_4(NbOF_5)_2]$ are shown in Figures 5 and 6, respectively. Very broad ^{93}Nb static NMR resonances were observed (Figures 5a and 6a), which result from large quadrupolar and chemical shift interactions. Niobium-93 MAS NMR spectra obtained at spinning speeds of 20 kHz at field strengths of 8.5 T are shown in Figures 5b and 6b. C_Q, η, and δ_{iso} are very difficult to extract from these spectra, due to the severe overlap between spinning sidebands and centerband. Examination of the spectra collected under ultrahigh spinning speeds (43 kHz) at an ultrahigh magnetic field strength (19.6 T) (Figures 5c and 6c) reveals that although the sidebands are now separated from the centerband, a large CSA dominates the spectra, due to the high field strength, resulting in a significant contribution of the central transition to the spinning sidebands.

Simulation of ^{93}Nb NMR Spectra: Methodology. We have used a similar approach to that outlined in our earlier paper to analyze the ^{93}Nb spectra.[12] A general equation that describes the appearance of the central transition of the quadrupolar nucleus with large quadrupolar and CS interactions under static conditions can be written:[20−24]

$$\nu_{1/2\leftrightarrow -1/2} = \nu_0 + \nu_Q^{(2)}(\theta, \phi) - \nu_{CS}(\theta, \phi, \alpha, \beta, \gamma) \quad (1)$$

where ν_0 is the Larmor frequency of the quadrupolar nucleus; θ and ϕ are polar and azimuthal angles, respectively, that define the orientation of the EFG tensor with respect to the applied magnetic field; and α, β, and γ are the Euler angles that define the orientation of the CS tensor with respect to the EFG tensor via the following rotational operations:[25]

$$R(\alpha, \beta, \gamma) = R_{Z''}(\gamma)R_{Y'}(\beta)R_Z(\alpha) \quad (2)$$

Explicit expressions for $\nu_Q^{(2)}$ and ν_{CS} have been given elsewhere.[23] Thus, the simulations of the static and MAS spectra acquired at low spinning frequencies are dependent on eight parameters: the quadrupolar parameters C_Q and η, the three principal components of the chemical shielding tensor (defined from least to most shielded, $\delta_{11} \geq \delta_{22} \geq \delta_{33}$), and the three Euler angles, α, β, and γ. The principal components of the EFG tensor are defined in this paper as $|V_{33}| \geq |V_{22}| \geq |V_{11}|$; C_Q is given by eQV_{33}/h, and the asymmetry parameter, η, is given by $(V_{11} - V_{22})/V_{33}$.

Simulation of the ^{93}Nb MAS NMR Spectra for a CS Interaction That Is Greater Than the Spinning Frequency. The spectra shown in Figure 5c and 6c reveal significant sideband manifolds (covering about a 3500 ppm range). The CS interactions of the niobium oxyfluorides are, clearly, much larger than that of K_2NbF_7.[11] It is not sufficient to simulate the centerband of the central transition, by only considering the quadrupolar parameters, since the spinning speed is insufficient to average the CS interaction completely. The time-dependent term due to the CS interaction only generates the first few, lower-order, sidebands. Thus, the first few sidebands and centerband can be summed to produce a line shape that can be simulated by average Hamiltonian theory under infinite spinning speed conditions, i.e., only the quadrupolar parameters need to be considered. The methodology to generate the spectrum that

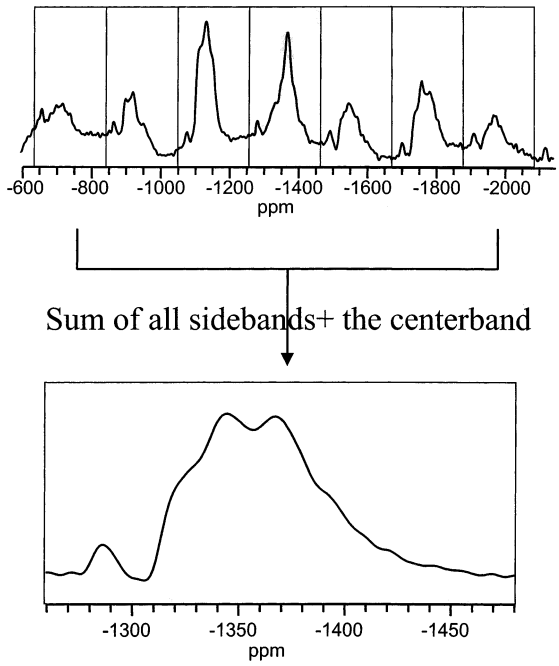

Figure 7. Methodology used to obtain a line shape for the simulations. The ^{93}Nb MAS spectrum of $Cdpy_4NbOF_5$ collected at 19.6 T, divided into units of the spinning speed (43 kHz), is shown on top. The central box contains the centerband of the central transition. The spectrum on the bottom represents the result of adding all the sidebands in each box to the centerband.

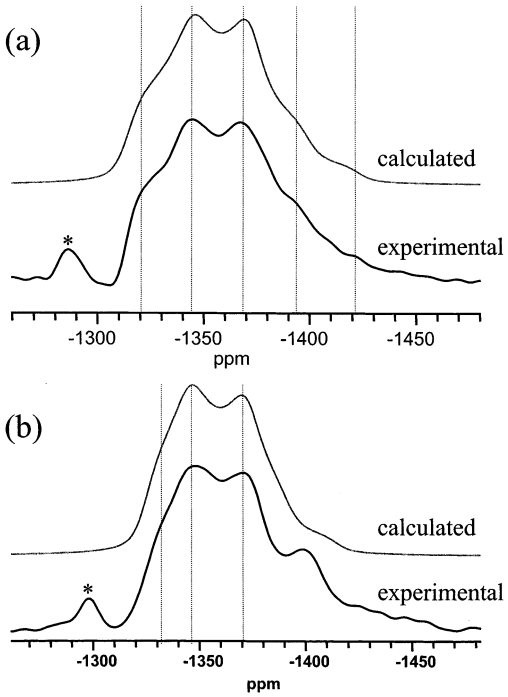

Figure 8. Experimental (lower) and simulated (upper) ^{93}Nb MAS NMR spectra of (a) $Cdpy_4NbOF_5$ and (b) $[pyH]_2[Cdpy_4(NbOF_5)_2]$, acquired at 19.6 T and $\nu_r = 43$ kHz. The experimental spectra were obtained from the treatment shown in Figure 7. The simulated spectra (panel a/panel b) were calculated with the following parameters: $C_Q = 36.0(5)/33.2(5)$ MHz, $\eta = 0.50(5)/0.40(5)$, and $\delta_{iso} = -1310(10)/-1320(10)$ ppm. The asterisks denote satellite transitions. The vertical dashed lines shown in this and subsequent spectra have been added to allow the positions of the discontinuities in the experimental and calculated spectra to be compared.

mimics that acquired under infinitely fast MAS conditions is shown in Figure 7. The spectrum in the central box, shown on the top of Figure 7, is the centerband of the central transition. The spectrum calculated by adding the first three sidebands into the centerband of the central transition, shown on the bottom of Figure 7, reveals a typical line shape broadened by the second-order quadrupolar interaction, which can now be readily simulated since it is dependent on only three parameters (Figure 8a,b). The simulated (upper) spectra were calculated with $C_Q = 36.0(5)$ and 33.2(5) MHz, $\eta = 0.50(5)$ and 0.40(5), and $\delta_{iso} = -1310(10)$ and $-1320(10)$ ppm for $Cdpy_4NbOF_5$ and $[pyH]_2[Cdpy_4(NbOF_5)_2]$, respectively. The differences between the simulated and experimental spectra of $[pyH]_2[Cdpy_4(NbOF_5)_2]$ (Figure 8b) may be due to an impurity resonance at ca. -1400 ppm.

Simulation of ^{93}Nb NMR Spectra of Stationary Samples: Niobium Chemical Shielding Anisotropy. Since the quadrupolar parameters were estimated from the simulations of the spectra collected at ultrahigh field and spinning speeds, the number of variable parameters needed to simulate the static spectra acquired at 8.5 T can be reduced, with only the CS tensor and its relative orientation with respect to the EFG tensor remaining as adjustable parameters. Simulations of the ^{93}Nb static NMR spectra of $Cdpy_4NbOF_5$ and $[pyH]_2[Cdpy_4(NbOF_5)_2]$ are shown in Figure 9, panels a and b, respectively. The experimental spectra acquired at 8.5 T with ^{19}F decoupling are shown as the bottom traces; the calculated spectra including the CSA and the calculated spectra without the CSA are depicted as solid and dotted upper traces, respectively. It is apparent that the contribution of the CSA to the line shape is significant. For instance, the contribution of the CSA to the overall breadth of the spectra is roughly 100 kHz at 8.5 T, which represents 45% of the total width of the spectrum. This is the first example of a system where a very large chemical shielding interaction in ^{93}Nb NMR has been characterized. It is clear that if the chemical shift anisotropy is ignored in the simulations of these ^{93}Nb NMR spectra, the quadrupolar interaction will be overestimated.

The following parameters were determined for $Cdpy_4NbOF_5$ from the simulations: $C_Q = 36.0(5)$ MHz, $\eta = 0.50(2)$ and $\delta_{iso} = -1310(10)$ ppm. The span of the CS tensor, defined as $\Omega = \delta_{11} - \delta_{33}$, is 1000(20) ppm. The skew of the CS tensor, $\kappa = 3(\delta_{22} - \delta_{iso})/\Omega$, where $-1 \le \kappa \le 1$, is equal to 1.0(5), indicating that the CS tensor is axially symmetric. The largest component of the EFG tensor, V_{33}, was found to be coincident with the most shielded component of the CS tensor, δ_{33}. The parameters for $[pyH]_2[Cdpy_4(NbOF_5)_2]$ were also determined and the parameters obtained from the simulations for the two compounds are summarized in Table 1. A slightly larger CSA was found for $[pyH]_2[Cdpy_4(NbOF_5)_2]$ and V_{33} and δ_{33} are slightly off-coincident, which may result from the hydrogen-bonding between axial fluorine and the pyridinium ion.

Simulations of the Full ^{93}Nb MAS NMR Spectra. These spectra were simulated in order to provide additional confirmation of the parameters obtained from the high field/high spinning speed spectra. The simulations require input of both the EFG and CS tensors and their relative orientation, making these simulations difficult without some prior determination of the quadrupole parameters. The result of simulations on ^{93}Nb MAS NMR spectra of $Cdpy_4NbOF_5$ and $[pyH]_2[Cdpy_4(NbOF_5)_2]$ collected at a spinning speed of $\sim$43 kHz at 19.6 T are shown in Figure 10, panels a and b, respectively. The simulated spectra (upper trace in each panel) were calculated from the parameters listed in Table 1. Good fits are obtained for both the relative intensities of the sidebands and the lineshapes of each individual sideband. The differences in Figure 10b may result from impurities.

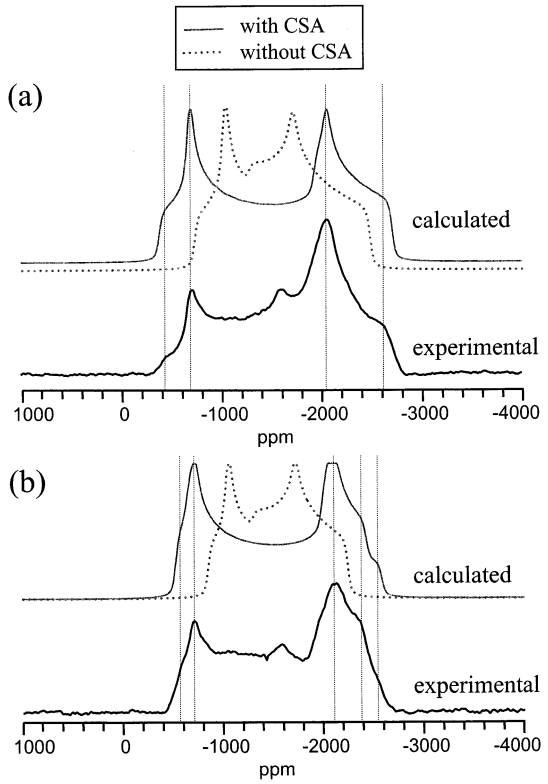

Figure 9. Experimental (lower) and simulated (upper) ^{93}Nb static NMR spectra of (a) $Cdpy_4NbOF_5$ and (b) $[pyH]_2[Cdpy_4(NbOF_5)_2]$, acquired at 8.5 T. The simulated (upper) spectra were calculated by including (solid lines) and ignoring (dashed lines) the CS tensor. Simulation parameters used (panel a/panel b) are $C_Q = 36.0(5)/33.2(5)$ MHz, $\eta = 0.50(5)/0.40(5)$, $\delta_{iso} = -1310(10)/-1320(10)$ ppm, $\Omega = 1000(20)/1100(20)$ ppm, $\kappa = 1.00(5)/0.80(5)$, $\alpha = 0(20)°/60(20)°$, $\beta = 0(2)°/5(2)°$, $\gamma = 0(20)°/0(20)°$.

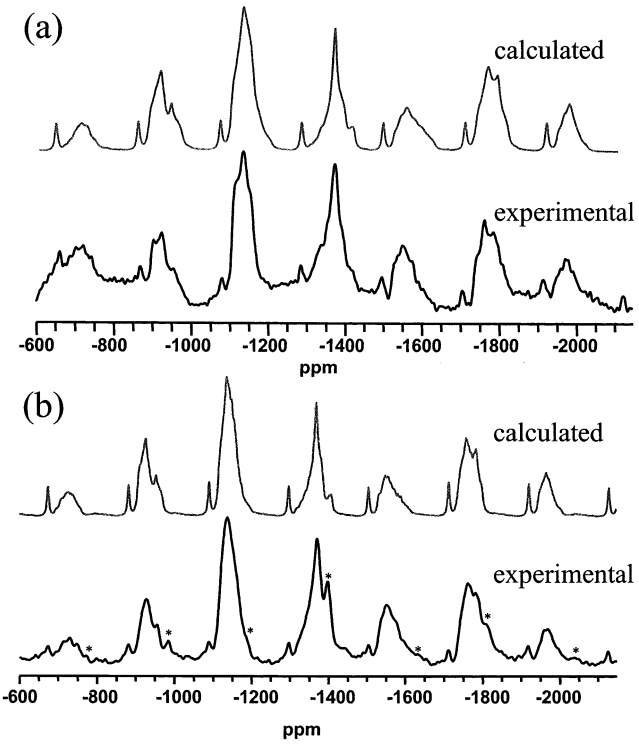

Figure 10. Experimental (lower) and simulated (upper) ^{93}Nb MAS NMR spectra of (a) $Cdpy_4NbOF_5$ and (b) $[pyH]_2[Cdpy_4(NbOF_5)_2]$, acquired at 19.6 T and $\nu_r = 43$ kHz. Simulation parameters (panel a/panel b): $C_Q = 36.0(5)/33.2(5)$ MHz, $\eta = 0.50(5)/0.40(5)$, $\delta_{iso} = -1310(10)/-1320(10)$ ppm, $\Omega = 1000(20)/1100(20)$ ppm, $\kappa = 1.00(5)/0.8(1)$, $\alpha = 0(20)°/60(20)°$, $\beta = 0(2)°/5(2)°$, $\gamma = 0(20)°/0(20)°$. Asterisks denote the peaks due to impurities.

The ^{93}Nb MAS spectra collected at lower spinning speed and lower field where sidebands and centerband overlap were also well reproduced (Figure 11). Although there are a few discrepancies in the relative intensities of parts of the spectra, most of the discontinuities in the calculated spectra match those in the experimental spectra. Since a Hahn echo was used to collect ^{93}Nb spectra at 8.5 T, the difference in transverse relaxation in the powder may result in errors in the intensities of parts of the experimentally determined line shapes. These simulations provide an important control, to check the validity of the parameters extracted from the previous simulations.

Simulations of ^{19}F MAS NMR: J-Coupling and Residual Dipolar Coupling between ^{93}Nb and ^{19}F. The ^{19}F MAS NMR spectra of niobium oxyfluorides acquired at 4.7 T contain asymmetric multiplets, resulting from *J*-coupling and residual dipolar coupling to the quadrupolar nucleus ^{93}Nb. Residual dipolar coupling arises from terms in the dipolar Hamiltonian, which cannot be averaged by MAS[26−29] and results in either increasing or decreasing spacings between the peaks in the multiplet, with increasing frequency. The problem has been treated by either first-order perturbation theory[30−32] or full diagonalization of combined Zeeman and quadrupolar Hamiltonians.[33,34] The former treatment is used for simulations of the ^{19}F MAS NMR spectra in this paper, and is valid in the limit where $C_Q/[4S(2S-1)] \ll \nu_0$, where ν_0 is the Larmor frequency of the quadrupolar nucleus. The frequencies of each of the peaks in the multiplet are shifted by both the *J*-coupling interaction and the residual dipolar shift, as given by

$$\nu_{m_S} = \nu_{iso} - m_S J_{iso} + \frac{S(S+1) - 3m_S^2}{S(2S-1)} d \qquad (3)$$

where ν_{m_S} is the frequency of the spin 1/2 *J*-multiplet that corresponds to the spin state, m_S, of the quadrupolar nucleus, ν_{iso} is the isotropic frequency, *S* is the spin of the quadrupolar nucleus, and *d* is the residual dipolar shift, which can be written as

$$d = \left(\frac{3C_Q R_{eff}}{20\nu_0}\right)[(3\cos^2\beta^D - 1) + \eta\sin^2\beta^D \cos 2\alpha^D] \qquad (4)$$

where R_{eff} is the effective dipolar coupling constant ($R_{eff} = R_{DD} - \Delta J/3$), R_{DD} is the dipolar coupling constant [$R_{DD} = (\mu_0/4\pi)(\gamma_I\gamma_S/2\pi)r_{IS}^{-3}$] and ΔJ is the anisotropy of the **J**-tensor ($\Delta J = J_{||} - J_{\perp}$). The **J** tensor is presumed to be axially symmetric with its unique axis directed along the bond vector, i.e., collinear with the dipolar tensor.[35] The angles β^D and α^D are the polar and azimuthal angles, which describe the orienta-

TABLE 1: Simulation Results for the ^{93}Nb Spectra of $Cdpy_4NbOF_5$ and $[PyH]_2[Cdpy_4(NbOF_5)_2]$, Obtained by Iterative, Simultaneous Fitting of All the ^{93}Nb Spectra

	C_Q (MHz)	η	δ_{iso}(^{93}Nb) (ppm)	Ω (ppm)	κ	α (deg)	β (deg)	γ (deg)
$Cdpy_4NbOF_5$	36.0 (5)	0.50 (2)	−1310 (10)	1000 (20)	1.00 (5)	*a*	0 (2)	*a*
$[pyH]_2[Cdpy_4(NbOF_5)_2]$	33.2 (5)	0.40 (2)	−1320 (10)	1100 (20)	0.80 (5)	60 (20)	5 (2)	0 (20)

[a] These values are undefined since $\beta = 0$.

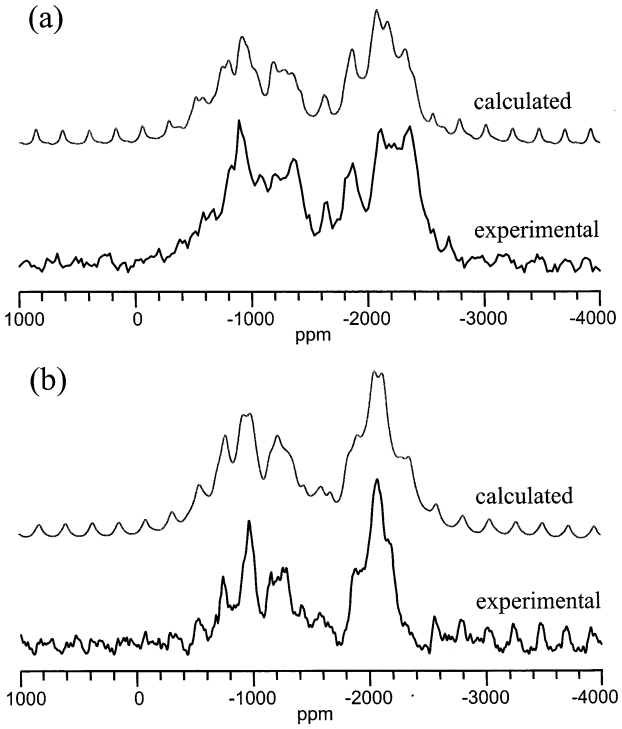

Figure 11. Experimental (lower) and calculated (upper) ^{93}Nb MAS NMR spectra of (a) $Cdpy_4NbOF_5$ and (b) $[pyH]_2[Cdpy_4(NbOF_5)_2]$, acquired at 8.5 T and $\nu_r = 10$ kHz. Calculation parameters (panel a/panel b): $C_Q = 36/33.2$ MHz, $\eta = 0.5/0.4$, $\delta_{iso} = -1310/-1320$ ppm, $\Omega = 1000/1100$ ppm, $\kappa = 1/0.8$, $\alpha = 0°/60°$, $\beta = 0°/5°$, $\gamma = 0°/0°$.

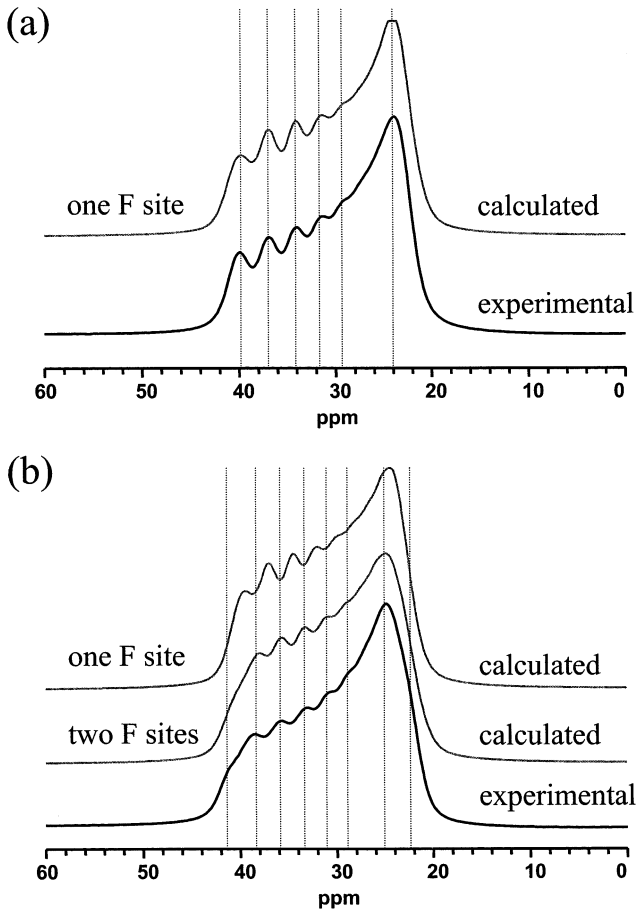

Figure 12. Experimental (lower) and calculated (upper) ^{19}F MAS NMR spectra of (a) $Cdpy_4NbOF_5$ and (b) $[pyH]_2[Cdpy_4(NbOF_5)_2]$, acquired at 4.7 T and $\nu_r = 24$ kHz. Calculation parameters (panel a): $C_Q = 36$ MHz, $\eta = 0.5$, $\delta_{iso} = -29.7(1)$ ppm, $J_{iso} = 362(2)$, $R^{DD} = 3860$ Hz, $\alpha^D = 0(5)°$, $\beta^D = 90(2)°$. Calculation parameters (panel b): $C_Q = 33.2$ MHz, $\eta = 0.4$, $J_{iso} = 350(5)$, $R^{DD} = 3850$ Hz, $\alpha^D = 0(5)°$, $\beta^D = 90(2)°$. $\delta_{iso} = -30.0$ ppm for the one-site simulation (top trace); $\delta_{iso} = -29.2(1)$ and $-31.0(1)$ ppm for the two-site simulation (middle trace).

tion of the dipolar vector with respect to the EFG tensor. The isotropic *J*-coupling can be measured from the splitting between the central peaks of the multiplet, which result from coupling to the $+1/2$ and $-1/2$ spin states of the niobium nucleus.

Simulations of the fast-spinning ^{19}F MAS NMR spectra were attempted with a variety of models, including a single ^{93}Nb, ^{19}F spin pair, and simulations including two different fluorine sites with different relative EFG orientations. The dipolar coupling constant R_{DD} (= 3850 Hz) was calculated from the average Nb−F(equatorial) distance.[1,2] Quadrupolar parameters utilized in these simulations were determined from analysis of the ^{93}Nb NMR spectra, reducing the number of parameters in these fits.

Since there are two crystallographically distinct fluorine sites involved in the multiplet at ca. 30 ppm, it is therefore surprising that fine structure is observed. From the simulation result of $Cdpy_4NbOF_5$, there appears to be a single isotropic ^{19}F chemical shift and a single *J*-coupling. This may be due to similar environments of equatorial fluorine atoms in the $NbOF_5$ octahedra. The experimental and calculated spectra of $Cdpy_4NbOF_5$ are shown in Figure 12a. The following parameters were determined by this simulation: $\delta_{iso}(^{19}F) = 29.7(1)$ ppm, $^1J(^{93}Nb,^{19}F) = 362(2)$ Hz, $\alpha^D = 0(5)°$, and $\beta^D = 90(2)°$. The result shows that the average Nb−F dipolar vector for the Nb−F(equatorial) bond is perpendicular to the largest component of the EFG tensor, V_{33}. Therefore, V_{33} is collinear with the O−Nb−F(axial) axis and points towards the unique O atom in the $NbOF_5$ octahedron.

A reasonable fit to the experimental spectrum of $[pyH]_2[Cdpy_4(NbOF_5)_2]$ could not be obtained when a single ^{93}Nb, ^{19}F spin pair was used (Figure 12b). A broader multiplet with broad shoulders on both sides was observed in the experimental spectrum of $Cdpy_4NbOF_5$. This implies that there is more than one fluorine site. The best fit to the experimental data was obtained by summing two similar multiplets with slightly different isotropic chemical shifts. The simulated spectrum based on this two-site model with equal intensities for each site is shown as the middle trace in Figure 12b and the following parameters were determined: $\delta_{iso}(^{19}F) = 28.9(1)$ and 30.6(1) ppm, $^1J(^{93}Nb,^{19}F) = 350(2)$ Hz, $\alpha^D = 0(5)°$, and $\beta^D = 90(2)°$. The dipolar coupling constant $R_{DD} = 3840$ Hz was again calculated from the average Nb−F(equatorial) distance and quadrupolar parameters obtained from the simulations of ^{93}Nb NMR spectra were used.

Interpretation of the ^{93}Nb MAS NMR NMR Spectra Collected under Ultrahigh Spinning Speeds and an Ultrahigh Field. As shown by Samoson et al.,[36] the shift $\delta^{(2)}$ and broadening $\Delta(m)$ caused by the second-order quadrupolar interaction are given by

$$\delta^{(2)}(m) = \frac{3}{40}\frac{{C_Q}^2}{{\nu_0}^2}\frac{I(I+1) - 9m(m-1) - 3}{I^2(2I-1)^2}\left(1 + \frac{\eta^2}{3}\right) \quad (5)$$

and

$$\Delta(m) = \frac{3}{128}\frac{{C_Q}^2}{{\nu_0}^2}\frac{6I(I+1) - 34m(m-1) - 13}{I^2(2I-1)^2}\left(1 + \frac{\eta^2}{3}\right) \quad (6)$$

TABLE 2: Relative Quadrupolar Shifts $\delta^{(2)}(m)$ and Broadening $\Delta(m)$ of the Satellite Transitions Caused by the Second-Order Quadrupolar Interaction, in Comparison to Those of Central Transition

m	1/2	3/2	5/2	7/2	9/2
$\delta^{(2)}(m)/\delta^{(2)}(m=1/2)$	1	0.625	−0.5	−2.375	−5
$\Delta(m)/\Delta(m=1/2)$	1	0.764	0.055	−1.125	−2.778

where I is the spin quantum number and $m = 1/2$ represents the central transition, $m = 3/2$ represents the satellite transitions between $m = \pm 1/2$ and $m = \pm 3/2$, etc. To interpret the spectra collected at ultrahigh fields and spinning speeds, the relative broadening and shifts of satellite transitions with respect to those of central transition were calculated on the basis of eqs 5 and 6 and are listed in Table 2. There are two important implications of these two equations: the $m = 5/2$ satellite transition for spin 9/2 nuclei has the smallest broadening, and only the quadrupolar shift of the $m = 3/2$ satellite transition has the same sign as that of the central transition. The $m = 7/2$ and 9/2 satellite transitions were not observed in our experimental spectra, since the intensities of sidebands are very small, due to not only the broad sideband distribution caused by the first-order quadrupolar interaction but also the broadening caused by the second-order quadrupolar interaction. The smaller broadening factors relative to that of the central transition (0.764 and 0.055 for $m = 3/2$ and 5/2, respectively) result in distinct sets of sidebands from the $m = 3/2$ and 5/2 satellite transitions, as shown in Figure 13.

A More Detailed Examination of the Effect of the Quadrupolar and CS Parameters on the Simulations of the Full ^{93}Nb MAS Spectra. Since the relative intensities and line shapes of the sidebands and centerband are controlled by the EFG and CS tensors and their relative orientation, it is feasible to refine the parameters by simulating the full spectrum. As shown in eqs 5 and 6, the broadening and shift depend mainly on C_Q, η, and m, the difference in the second-order quadrupolar induced shift between the central transition and satellite transitions depending on quadrupolar parameters C_Q and η. By carefully examining the positions of centerband of the central transition and sidebands due to satellite transitions (e.g., $m = 5/2$ for ^{93}Nb) in comparison to those of experimental spectrum, C_Q can be extracted. The effect of changing C_Q is shown in Figure 14. The centerband shifts to lower frequency significantly when C_Q becomes larger. On the other hand, the sidebands of the satellite transition for $m = 5/2$ slightly shift to higher frequency when C_Q increases. The breadths of the centerband and sidebands of the central transition also increase slightly when the size of the quadrupolar interaction increases. Considering the shift in hertz between the spectra calculated with $C_Q = 33$ and 39 MHz, the shift in position of the central transition is about −4000 Hz and the shift of the $m = 5/2$ satellite transition is about 1700 Hz. Thus, $\delta^{(2)}(5/2)/\delta^{(2)}(1/2) = -0.425$, which is roughly in agreement with the shift factor of −0.5 given in Table 2. The opposite direction of the second-order quadrupolar shifts of the central transition and this satellite transition leads to an increase in the sensitivity of the relative peak positions of these transitions to the quadrupolar interaction. The simulated spectra (upper traces) calculated with different values of η and the experimental spectrum (bottom trace) are depicted in Figure 15. η not only affects the quadrupolar shifts of the peaks but also affects the line shapes of the centerband and sidebands. Variations in η can cause significantly different spectra. The size and shape of the CS tensor mainly influences the relative intensities of the centerband and the first few sidebands. The relative orientation of the EFG and CS tensors,

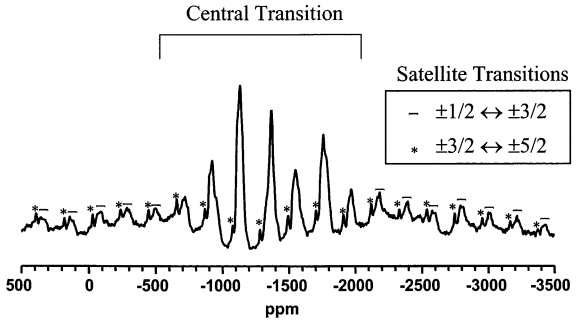

Figure 13. Assignments of the peaks in the ^{93}Nb MAS NMR spectrum of $Cdpy_4NbOF_5$ collected at 19.6 T and $\nu_r = 43$ kHz.

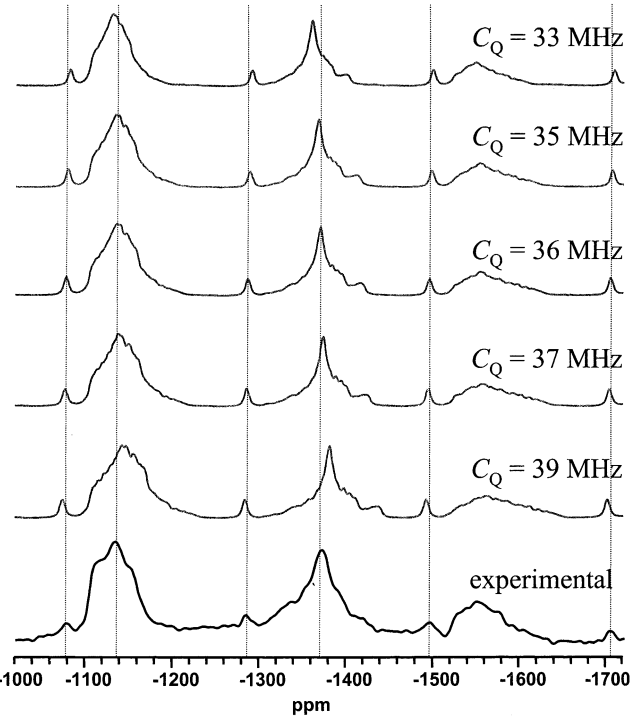

Figure 14. Effects of changing the size of EFG tensor (C_Q). Experimental (bottom trace) and calculated (upper traces) ^{93}Nb MAS NMR spectra of $Cdpy_4NbOF_5$ acquired at 19.6 T and $\nu_r = 43$ kHz. Simulation parameters: $C_Q = 33$, 35, 36, 37, and 39 MHz, $\eta = 0.5$, $\delta_{iso} = -1310$ ppm, $\Omega = 1000$ ppm, $\kappa = 1$, $\alpha = 0°$, $\beta = 0°$, $\gamma = 0°$.

however, strongly influences the line shapes of the centerband and the first few sidebands. The simulated spectra (upper traces) calculated with different values of β and the experimental spectrum (bottom trace) are shown in Figure 16. The line shapes are especially sensitive to the angle between the largest components of the two tensors, β, which provides for a very accurate estimation of β; this is reflected in the small errors listed for this parameter. The errors listed in Table 1 for the eight variables were determined by carefully varying each parameter independently and determining the effect of this on the positions of the discontinuities and the relative intensities of the different parts of the spectra and the various sidebands. The errors for C_Q, η, and δ_{iso} were first determined by careful simulation of the "infinite spinning" MAS spectra, which are dependent on these three parameters only. Given the extreme sensitivity of the full (i.e., satellite and central transition) MAS spectra on η, the error in the determination of this parameter could be reduced by simulation of these spectra. The errors in the determination of C_Q, as determined from both the full and central transition MAS spectra, were similar. C_Q, η, and δ_{iso} were fixed in the simulations of the static spectra, reducing the

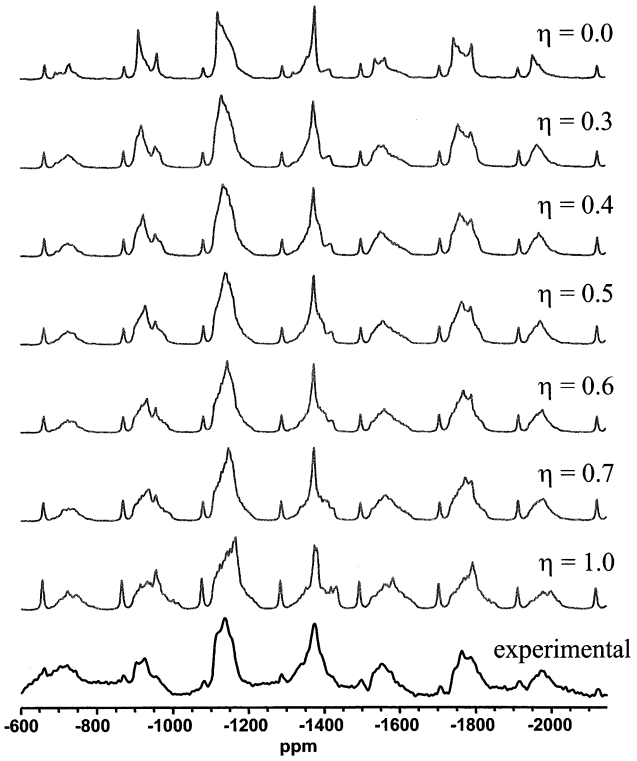

Figure 15. Effect of changing the asymmetry of the EFG tensor (η). Experimental (bottom trace) and calculated (upper traces) ^{93}Nb MAS NMR spectra of $Cdpy_4NbOF_5$ acquired at 19.6 T and $\nu_r = 43$ kHz. Simulation parameters: $\eta = 0.0$, 0.3, 0.4, 0.5, 0.6, 0.7, and 1.0, $C_Q = 36$ MHz, $\delta_{iso} = -1310$ ppm, $\Omega = 1000$ ppm, $\kappa = 1$, $\alpha = 0°$, $\beta = 0°$, $\gamma = 0°$.

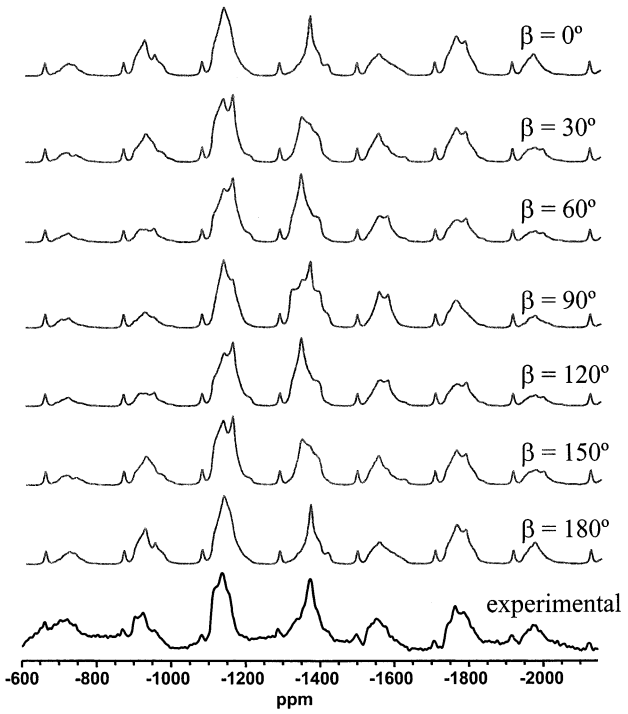

Figure 16. Effects of changing the relative orientation of the CS tensor with respect to the EFG tensor (β). Experimental (bottom trace) and calculated (upper traces) ^{93}Nb MAS NMR spectra of $Cdpy_4NbOF_5$ acquired at 19.6 T and $\nu_r = 43$ kHz. Simulation parameters: $\beta = 0°$, 30°, 60°, 90°, 120°, 150°, and 180°, $C_Q = 36$ MHz, $\eta = 0.5$, $\delta_{iso} = -1310$ ppm, $\Omega = 1000$ ppm, $\kappa = 1$, $\alpha = 0°$, $\gamma = 0°$.

number of independent parameters, and ensuring that sufficient (3D) parameter space (5D for the second compound) was explored in the simulations to provide accurate estimates of the errors. This also ensured that an alternative set of parameters, that could provide an equally good fit, were not overlooked or missed.

Discussion

Disorder in $[pyH]_2[Cdpy_4(NbOF_5)_2]$. Two ^{19}F resonances were found in $Cdpy_4NbOF_5$ and originate from equatorial and axial fluorine sites, while four resonances were found in $[pyH]_2[Cdpy_4(NbOF_5)_2]$, two of which originate from axial fluorine sites and the other two from the equatorial sites. The splitting of the fluorine resonances belonging to the axial and equatorial fluorine sites may be due to the disorder in the orientation of the pyridinium ions.[2] Larger splittings are seen for the axial fluorine resonances than for the equatorial fluorine resonances (12 ppm vs 2 ppm), supporting the above interpretation, since the pyridinium ion is closer to the axial fluorine sites.

^{19}F Chemical Shifts of Niobium Fluorides. Very distinct chemical shifts are observed for fluorine atoms coordinated to niobium, depending on the nature of the atom trans to the fluorine atom. For example, a shift of −136 ppm was observed in our earlier work for K_2NbO_3F, a compound containing NbO_5F octahedra.[11] This shift is close to those observed for the terminal (or axial) fluorine atoms in the NbF_5O octahedra studied in this work. In contrast, the fluorine atoms in NbF_7^{2-} anions resonate at +76 ppm,[12] in the same chemical shift range as the equatorial fluorine atoms in the NbF_5O octahedra. The large shift to negative frequencies for trans O−Nb−F fluorine is ascribed to the strong coordination between oxygen and the Nb t_{2g} orbitals, which should reduce the strength of the Nb−F bonds.

(a)

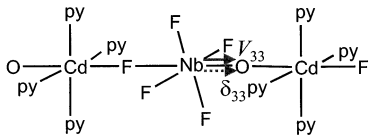

(b)

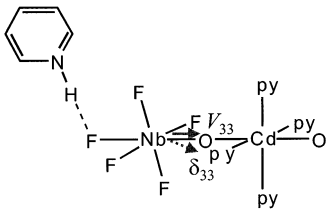

Figure 17. Orientations of the principal components of the EFG and CS tensors, V_{33} and δ_{33}, in (a) $Cdpy_4NbOF_5$ and (b) $[pyH]_2[Cdpy_4(NbOF_5)_2]$.

Relative Orientation between Tensors. Since the relative orientations between the ^{19}F−^{93}Nb dipolar vector and ^{93}Nb EFG tensor and between the CS tensor and EFG tensor were determined, the possible orientations of the largest components of the tensors can therefore be predicted and are shown in Figure 17, panels a and b for $Cdpy_4NbOF_5$ and $[pyH]_2[Cdpy_4(NbOF_5)_2]$, respectively. V_{33} and δ_{33} of $Cdpy_4NbOF_5$ are collinear and perpendicular to Nb−F(equatorial) and point toward the oxygen. This is reasonable since the unique axis is along the Nb−O bond in the $NbOF_5$ octahedron. δ_{33} for $[pyH]_2[Cdpy_4(NbOF_5)_2]$ lies slightly off the Nb−O axis (Figure 17b). This change in orientation may be caused by small changes in the local electronic environment caused by the hydrogen-bonding interaction between the pyridinium and the axial fluorine ions.

***C*$_Q$(^{93}Nb).** On the basis of the reported C_Q(^{93}Nb) values of hexacoordinate niobium atoms at room temperature, the C_Q(^{93}Nb) values of 36.0 and 33.2 MHz, measured for $NbOF_5$ octahedra in oxyfluoroniobates, lie in the intermediate range of niobium quadrupole coupling constants, with very small C_Q(^{93}Nb) on the order of hundreds of kilohertz for NbO_2F[37] and in $Nb(OMg)_6$ octahedra in PMN,[38] and larger C_Q(^{93}Nb) values of 19.5 and 22 MHz in NbO_6 octahedra in $NaNbO_3$[39] and $LiNbO_3$[40], respectively, and very large C_Q(^{93}Nb) values of >62 MHz in $Nb(ONb)_{6-x}(OMg)_x$ octahedra in PMN.[38] The larger C_Q(^{93}Nb) results from the more distorted niobium octahedron. The anomalously small value of C_Q(^{93}Nb) observed for NbO_2F may be due to the presence of thermal motion, which could result in a smaller C_Q(^{93}Nb). This behavior has previously been observed in solid-state NMR experiments of $NaNbO_3$[41] and K_2NbF_7.[12]

^{93}Nb CSA and *J*-Coupling. The simulations of ^{93}Nb NMR static spectra of the oxyfluoroniobates reveal a very significant niobium CSA ($\Omega \sim 1000$ ppm) in these compounds. The CSA is considerably larger than the value determined in our previous study of K_2NbF_7 ($\Omega \sim 200$ ppm). The measured values of ^1J(^{93}Nb,^{19}F) for the out-of-center distorted hexacoordinate compounds are slightly larger than the values of ^1J(^{93}Nb,^{19}F) reported for the octahedral and pentahedral niobium fluoride complexes from ^{19}F solution NMR experiments on NbF_6^-, ^1J(^{93}Nb, ^{19}F) = 345 Hz,[42] and $NbF_5 \cdot 2(CH_3)_2SO$, ^1J(^{93}Nb, ^{19}F) = 335 Hz,[43] and is larger than the value of ^1J(^{93}Nb,^{19}F) = 204 Hz[12] for heptacoordinate niobium fluoride, K_2NbF_7.

Site Symmetries. The Nb sites in $Cdpy_4NbOF_5$ and $[pyH]_2[Cdpy_4(NbOF_5)_2]$ are located on centers of inversion and a C_2 axis, respectively, although O/F ordering in $Cdpy_4NbOF_5$ will remove this center of inversion, locally. The results of simulations show that the EFG tensors are not axially symmetric (η = 0.5 and 0.4), but the CS tensors are close to being axially symmetric. The EFG is a long-range interaction and is controlled by the arrangements of charges surrounding the central nucleus; thus this tensor is not expected to be axially symmetric. In contrast, the CS is influenced by the local arrangements of electrons and is not expected to be so strongly influenced by long-range effects. Thus, this near-axial symmetry of the CS tensor reflects the close to C_4 symmetry of the out-of-center $NbOF_5$ octahedra, if the surrounding atoms are ignored. The two compounds do not display ferroelectricity due to the long-range cancellation of the ferroelectric response caused by the pseudoinversion symmetry. We note, however, that solid-state NMR provides a measure of the local distortions of the octahedra and provides a measure of the size of the distortion that might be expected if materials with similar Nb−O/ F−Cd chains could be synthesized in noncentrosymmetric space groups.

Conclusions

The local structures of two niobium oxyfluorides have been studied with ^{113}Cd, ^{19}F, and ^{93}Nb MAS NMR. ^{113}Cd MAS NMR spectra of $Cdpy_4NbOF_5$ are consistent with an O/F ordering scheme that allows the acentric $NbOF_5$ octahedron to occupy a center of inversion in the crystal structure of $Cdpy_4NbOF_5$, by an interchain cancellation of the local reduction in symmetry due to O/F ordering. ^{19}F MAS NMR is also consistent with O/F ordering. A doubling in the number of resonances in the ^{19}F spectrum of $[pyH]_2[Cdpy_4(NbOF_5)_2]$, as compared to $Cdpy_4NbOF_5$, was observed, which was ascribed to disorder in the positions of the pyridinium ions that are hydrogen-bonded to the axial fluorine atoms in $Cdpy_4(NbOF_5)_2$.

We have presented a methodology for extracting the quadrupolar parameters in systems containing both large quadrupolar and chemical shielding interactions. This paper demonstrates the importance of NMR experiments conducted under ultrahigh spinning speed and ultrahigh magnetic field for extracting quadrupolar parameters from nuclei with very large quadrupolar and/or chemical shielding interactions ($C_Q \sim 35$ MHz, $\Omega \sim 1000$ ppm). A combination of ^{93}Nb and ^{19}F solid-state NMR experiments on spinning and stationary samples has provided correlations between NMR interaction parameters and local structure.

The large C_Qs and nonzero asymmetry parameters correspond to asymmetric, hexacoordinate environments about the niobium atoms in these materials. The magnitudes of C_Q(^{93}Nb) are found to lie between known values of C_Q in NbO_6 octahedral (ca. 20 MHz) and very distorted $Nb(ONb)_{6-x}(OMg)_x$ octahedral (>62 MHz) arrangements. Despite the large quadrupolar-dominated static powder patterns, a significant contribution to the line shape from anisotropic chemical shielding interactions is observed. This is the first report of such a large CSA ($\Omega = 1000$ ppm) in a ^{93}Nb system. Fluorine-19 fast MAS NMR experiments have allowed ^1J(^{93}Nb, ^{19}F) to be measured in the solid state. A very asymmetric multiplet due to the residual dipolar coupling between ^{93}Nb and ^{19}F was observed.

The ^{93}Nb MAS spectra were simulated numerically. The opposite signs of the second-order quadrupolar shifts of the central and $|\pm 3/2\rangle \leftrightarrow |\pm 5/2\rangle$ satellite transitions for spin 9/2 nuclei allows more accurate estimates of the quadrupolar parameters to be made, by simulating spectra in which the central and satellite transition sidebands are well separated. The relative orientation between the EFG and the CS tensor also contributes significantly to the line shapes of the centerband and sidebands in the simulations, resulting in more reliable measurements of these parameters.

Acknowledgment. This research was supported by a grant from the National Science Foundation (DMR9901308). Support of the National High Magnetic Field Laboratory (NHMFL) via the National Science Foundation Cooperative Agreement DMR-9527035 and by the State of Florida is gratefully acknowledged. We thank Professor K. R. Poppelmeier and Dr. K. R. Heier for helpful discussions and for supplying the materials used in this study. Dr. A. Samoson and Dr. T. Tuherm are gratefully acknowledged for assistance in the acquisition of solid-state NMR spectra at 19.6 T with their ultrahigh spinning speed probe. Dr. Z. Gan is thanked for helpful discussions.

References and Notes

(1) Halasyamani, P. S.; Heier, K. R.; Norquist, A. J.; Stern, C. L.; Poeppelmeier, K. R. *Inorg. Chem.* **1998**, *37*, 369−371.

(2) Halasyamani, P.; Willis, M. J.; Heier, K. R.; Stern, C. L.; Poeppelmeier, K. R. *Acta Crystallogr.* **1996**, *C52*, 2491−2493.

(3) Munowitz, M.; Jarman, R. H.; Harrison, J. F. *Chem. Mater.* **1993**, *5*, 661.

(4) Halasyamani, P.; Willis, M. J.; Stern, C. L.; Lundquist, P. M.; Wong, G. K.; Poeppelmeier, K. R. *Inorg. Chem.* **1996**, *35*, 1367−1371.

(5) Matthias, B. T.; Remeika, J. P. *Phys. Rev.* **1949**, *76*, 1886.

(6) Rocha, J.; Brandão, P.; Lin, Z.; Esculcas, A. P.; Ferreira, A. *J. Phys. Chem.* **1996**, *100*, 14978−14983.

(7) Gabuda, S. P.; Zil'berman, B. D.; Goncharuk, V. K. *Zh. Strukt. Khim.* **1978**, *19*, 431−441.

(8) Wheeler, R. A.; Whangbo, M. H.; Hughbanks, T.; Hoffman, R.; Burdett, J. K.; Albright, T. A. *J. Am. Chem. Soc.* **1986**, *108*, 2222.

(9) Heier, K. R.; Poeppelmeier, K. R. *J. Solid State Chem.* **1997**, *133*, 576−579.

(10) Fuller, G. H. *J. Phys. Chem. Ref. Data* **1976**, *5*, 835.

(11) Du, L.-S.; Wang, F.; Grey, C. P. *J. Solid State Chem.* **1998**, *140*, 285−294.

(12) Du, L.-S.; Schurko, R. W.; Lim, K. H.; Grey, C. P. *J. Phys. Chem. A* **2001**, *105*, 760−768.
(13) Wang, F.; Grey, C. P. *J. Am. Chem. Soc.* **1995**, *117*, 6637−6638.
(14) Wang, F.; Grey, C. P. *J. Am. Chem. Soc.* **1998**, *120*, 970−980.
(15) Du, L.-S.; Samoson, A.; Tuherm, T.; Grey, C. P. *Chem. Mater.* **2000**, *12*, 3611−3616.
(16) Alderman, D. W.; Solum, M. S.; Grant, D. M. *J. Chem. Phys.* **1986**, *84*, 3717.
(17) Eden, M.; Lee, Y. K.; Levitt, M. H. *J. Magn. Reson.* **1996**, *120*, 56.
(18) Charpentier, T.; Fermon, C.; Virlet, J. *J. Magn. Reson.* **1998**, *132*, 181.
(19) Smith, S. A.; Levante, T. O.; Meier, B. H.; Ernst, R. R. *J. Magn. Reson.* **1994**, *106a*, 75−105.
(20) Baugher, J. F.; Taylor, P. C.; Oja, T.; Bray, P. J. *J. Chem. Phys.* **1969**, *50*, 4914.
(21) Taylor, P. C.; Baugher, J. F.; Kriz, H. M. *Chem. Rev.* **1975**, *75*, 203.
(22) Cheng, J. T.; Edwards, J. C.; Ellis, P. D. *J. Phys. Chem.* **1990**, *94*, 553.
(23) Power, W. P.; Wasylishen, R. E.; Mooibroek, S.; Pettitt, B. A.; Danchura, W. *J. Phys. Chem.* **1990**, *94*, 591.
(24) Koons, J. M.; Hughes, E.; Cho, H. M.; Ellis, P. D. *J. Magn. Reson. A* **1995**, *114*, 12.
(25) Zare, R. N. *Understanding Spatial Aspects in Chemistry and Physics*; John Wiley & Sons: New York, 1988.
(26) Harris, R. K.; Olivieri, A. C. *Prog. Nucl. Magn. Reson. Spectrosc.* **1992**, *24*, 435.
(27) Harris, R. K. In *Encyclopedia of Nuclear Magnetic Resonance*; Grant, D. M., Harris, R. K., Eds.; John Wiley & Sons: Chichester, U.K., 1996; pp 2909−2914.
(28) McDowell, C. A. In *Encyclopedia of Nuclear Magnetic Resonance*; Grant, D. M., Harris, R. K., Eds.; John Wiley & Sons: Chichester, U.K., 1996; pp 2901−2908.
(29) Grondona, P.; Olivieri, A. C. *Concepts Magn. Reson.* **1993**, *5*, 319−339.
(30) Olivieri, A. C.; Frydman, L.; Diaz, L. E. *J. Magn. Reson.* **1987**, *75*, 50.
(31) Apperly, D. C.; Haiping, B.; Harris, R. K. *Mol. Phys.* **1989**, *68*, 1277.
(32) Olivieri, A. C. *J. Magn. Reson.* **1989**, *81*, 201.
(33) Menger, E. M.; Veeman, W. S. *J. Magn. Reson.* **1982**, *46*, 257.
(34) Alarcón, S. H.; Olivieri, A. C.; Harris, R. K. *Solid State Nucl. Magn. Reson.* **1993**, *2*, 325.
(35) Wasylishen, R. E. In *Encyclopedia of Nuclear Magnetic Resonance*; Grant, D. M., Harris, R. K., Eds.; John Wiley & Sons: Chichester, U.K., 1996; pp 1685−1695.
(36) Samoson, A.; Lippmaa, E.; Pine, A. *Mol. Phys.* **1988**, *65*, 1013.
(37) Man, P. P.; Theveneau, H.; Papon, P. *J. Magn. Reson.* **1985**, *64*, 271.
(38) Fitzgerald, J. J.; Prasad, S.; Huang, J.; Shore, J. S. *J. Am. Chem. Soc.* **2000**, *122*, 2556−2566.
(39) Meadows, M. D.; Smith, K. A.; Kinsey, R. A.; Rothgeb, T. M.; Skarjune, R. P.; Oldfield, E. *Proc. Natl. Acad. Sci. U.S.A.* **1982**, *79*, 1351.
(40) Peterson, G. E.; Bridenbaugh, P. M. *J. Chem. Phys.* **1968**, *48*, 3402.
(41) Wolf, F.; Kline, D.; Story, H. S. *J. Chem. Phys.* **1970**, *53*, 3538.
(42) Hatton, J. V.; Saito, Y.; Schneider, W. G. *Can. J. Chem.* **1965**, *43*, 47.
(43) Moss, K. C. *J. Chem. Soc. A* **1970**, 1224.